THE JOURNAL OF PHYSICAL CHEMISTRY C

Article

pubs.acs.org/JPCC

Water Transport Properties of Poly(butylene succinate) and Poly[(butylene succinate)-*co*-(butylene adipate)] Nanocomposite Films: Influence of the Water-Assisted Extrusion Process

Sébastien Charlon,[†] Nadège Follain,*[,†] Jérémie Soulestin,[‡] Michel Sclavons,[§] and Stéphane Marais*[,†]

[†]Normandie Univ, UNIROUEN, INSA Rouen, CNRS, PBS, 76000 Rouen, France

[‡]Department of Polymers and Composites Technology and Mechanical Engineering, Mines Douai, 941 rue Charles Bourseul, CS 10838, 59508 Douai, France

[§]Bio and Salt Matter, Institute of Condensed Matter and Nanosciences, Université Catholique de Louvain-la-Neuve, Croix du Sud 1, B-1348 Louvain-La-Neuve, Belgium

ABSTRACT: Poly(butylene succinate) (PBS) and poly[(butylene succinate)-*co*-(butylene adipate)] (PBSA)-based composite films loaded with 5 wt % of fillers (native or organo-modified montmorillonites) were extruded using a standard protocol or assisted by water injection. In the resulting composite films, the filler morphology was altered, as evidenced by TEM images. The CNa aggregates were broken with the help of water injection, and the exfoliation/dispersion levels of C30B were dependent on the matrix. By considering the degree of crystallinity of the polymer matrix, the nature of the fillers, and also the processing conditions, the film (micro)structure was successfully correlated to the water (liquid and vapor) behavior of the PBS- and PBSA-based films, studied by means of sorption and permeation measurements. The water permeability and diffusivity were significantly reduced even with an increased water sorption, depending on the matrix and the clay morphology or nature. Specifically, concomitant effects such as tortuosity and trapping but also preferential diffusion pathways as well as free volumes in matrix strikingly were responsible for the barrier performances evolution.

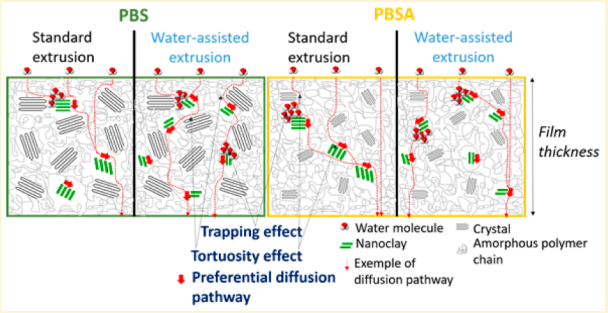

1. INTRODUCTION

Biodegradable polymers are currently developed because of their great interests, especially for biomedical applications,[1,2] to limit the number of surgical operations, and for packaging applications,[3,4] with the purpose of reducing the plastic pollution induced by the widely used nonbiodegradable polyolefins. In the latter case, the main challenge is focused on the elaboration of biopolymers having properties competitive to those of polyolefins. Poly(butylene succinate) (PBS) and poly[(butylene succinate)-*co*-(butylene adipate)] (PBSA) appear as promising biopolyesters. Indeed, they exhibit numerous advantages because they can be produced from renewable resources;[5] they are considered as biodegradable[6] and biocompatible.[7] In addition, they present a good processability[8] as well as good mechanical[9] and thermal properties,[10] which make them suitable for food packaging applications.[11] However, they are found too soft with a poor gas and moisture resistance.[12] In the field of barrier applications, one way to improve the barrier properties of a polymer is related to the incorporation of inorganic lamellar fillers allowing to reduce the diffusivity of permeant molecules, which occurs in the amorphous phase of the polymer, by inducing tortuosity effects.[13,14] Many papers related the strong dependence on tortuosity effects of dispersion and exfoliation levels of fillers into the polymer matrix.[15−17]

Taking advantage of the preparation of nanocomposite films, 5 wt % of inorganic clays (native and organo-modified montmorillonites) has been loaded in PBS and PBSA matrices using a recent process, called water-assisted extrusion process, based on the injection of liquid water under high conditions of temperature and pressure in the high compression zone of the extruder barrel during process. This original process is applied because it is reported to be active in increasing dispersion and exfoliation levels of nanofillers into the polymer matrices, as already demonstrated[18] with PP,[19,20] PA6,[21] and SAN[22] matrices.

The aim of the present work is to investigate in detail the water barrier properties of the resulting films presenting dispersion and exfoliation levels of fillers depending on the polyester matrix and on the process conditions. In fact, the two polymers are characterized by distinct degrees of crystallinity (57% and 37% for PBS and PBSA, respectively[23]). Cloisite Na^+ and Cloisite 30B as native and organo-modified montmor-

Received: November 3, 2016
Revised: December 14, 2016
Published: December 20, 2016

ACS Publications © 2016 American Chemical Society

DOI: 10.1021/acs.jpcc.6b11077
J. Phys. Chem. C 2017, 121, 918−930

illonites were selected and two extrusion processes were applied to elaborate the composite films; the standard extrusion process (i.e., without water injection) was used as a comparative technique to the water-assisted extrusion process. Water permeation and water vapor sorption measurements were performed on both unfilled and filled films in order to highlight the interactions occurring between polymer chains and nanofillers and those between water molecules themselves, which both depend on the matrix used. Only a few papers have reported the permeability to gases of PBS- and PBSA-based films.[24,25] Indeed, the transport of water molecules in PBS- and PBSA-based films correlated with clay morphology into the matrix is an original work as never reported in the literature to our knowledge. New experimental insights into water barrier properties were emphasized and were directly related to the difference in polymer crystallinity, the filler morphology, and the processing conditions used to elaborate the PBS- and PBSA-based composite films. In addition, specific effects, like tortuosity effects, trapping effects, and preferential diffusion pathways leading to percolation phenomenon, were pointed out to explain the change in water permeability, diffusivity, and solubility coefficients resulting from the use of water vapor and liquid water as diffusing species in sorption and permeation measurements.

2. EXPERIMENTAL SECTION

2.1. Materials. Poly(butylene succinate) (PBS) and poly[(butylene succinate)-*co*-(butylene adipate)] (PBSA) pellets were supplied by Natureplast (France) under the trade names PBE003 and PBE001, respectively. PBSA is a random copolymer having 21 ± 1 mol % of butylene adipate group, as attested by ^{1}H NMR.

Native montmorillonite (Cloisite Na^+, noted CNa) and organo-modified montmorillonite (Cloisite 30B, noted C30B) were supplied by BYK Additive (Germany). C30B is obtained after organo-modification of CNa with 30 wt % of a methylbis(2-hydroxyethyl) tallow alkylammonium.

2.2. Elaboration of Composite Films. Composite films were elaborated in three steps in order to optimize the dispersion and exfoliation levels of the nanoclays in PBS and PBSA matrices, as described by Soulestin et al.[26] Before processing, the polymer pellets were oven-dried at 70 °C for 15 h while inorganic fillers were used as received with the aim of maximizing their dispersion and exfoliation in the polymer films, as recently demonstrated by Tenn et al.[27] For the first step of preparing a masterbatch, polymer pellets and 15 wt % of inorganic clays were initially melt mixed into a Clextral BC45 twin-screw extruder having a ratio between the screw length L' and the screw diameter D equal to 22. The temperature profile of the screw was adjusted from 120 to 160 °C between the feed and the die. The throughput was fixed at 10 kg h^{-1}, and the screw speed at 110 rpm. The strands were cooled down into liquid water and pelletized. The obtained composites pellets were quickly oven-dried at 70 °C for 15 h to avoid polymer chains hydrolysis. Then, in order to prepare composites containing 5 wt % of fillers, the dried composite pellets were melt-mixed with neat polymer pellets using a corotating twin-screw extruder Krupp WP ZSK25 having a L'/D ratio equal to 40 with a temperature profile from 120 to 160 °C between the feed and the die for the PBS-based samples and from 120 to 180 °C for the PBSA-based samples. The throughput was adjusted to 8 kg h^{-1} and the screw speed to 400 rpm. At this step, it was possible to inject liquid water into the high compression zone of the extruder barrel with a pressure about 20−30 bar and a throughput equal to 2.4 kg h^{-1} for the PBS-based samples and to 1.8 kg h^{-1} for the PBSA-based samples as reported in a separate paper.[23] At the die, the strands were again cooled down into liquid water and pelletized. After a drying step at 70 °C for 15 h, the 5 wt %-loaded composites pellets were transformed into films using a calendaring extrusion process with a single-screw Haake Thermo extruder having a L'/D ratio equal to 40. The temperature profiles were fixed from 120 to 150 °C for the PBS-based samples and from 120 to 135 °C for the PBSA-based samples between the feed and the die. Each film is referenced as follows: polymer matrix + filler (weight percentage) for samples elaborated without water injection and polymer matrix + filler (weight percentage) − *W* for samples extruded with water injection.

2.3. Structure Analysis. *2.3.1. Gel Permeation Chromatography.* Average molecular weights of PBS and PBSA chains were measured at 27.5 °C using a PL-GPC 50 plus spectrometer from Varian (USA) equipped with a PLgel 5 μm mixed-C column. A 1 mL min^{-1} flux of dichloromethane was used as solvent, and a range of polystyrene standards were used for calibration. Preliminary, the composite films were dissolved in dichloromethane, and the resulting solutions were filtered two times on a filter having 0.45 μm pore size to remove fillers particles. Each measurement was duplicated.

2.3.2. Transmission Electron Microscopy. The dispersion and exfoliation levels of fillers in the PBS and PBSA matrices were observed using a LEO 922 transition electron microscope from Zeiss (Germany) with an acceleration tension adjusted to 200 kV. Samples were precut with a cryo-microtome Reichert with temperatures fixed at −30 and −40 °C for the film and for the knife, respectively. Ultrathin sections of approximately 95 nm thick were obtained with a cryo-diamond knife from Diatome (Switerland) using a cut angle of 35° and were then transferred to 400 mesh copper grid.

2.3.3. X-ray Diffraction. A Bruker AXS D8 Advance diffractometer equipped with a cobalt Kα radiation source (λ = 1.789 Å) was carried out with a current of 40 mA and a voltage of 35 kV. Measurements were performed by varying the 2θ angles between 2° and 14° with an angle increment equal to 0.04°/step in order to evaluate the basal distance of nanoplatelets in the intercalated structures.

2.4. Transport Properties. Before measurements, the films were dried under vacuum using P_2O_5 powder as moisture sorbent.

2.4.1. Water Permeation. Liquid water permeation measurements were performed at 25 °C using a homemade apparatus called "permeadiffusiometer", as already described by Alexandre et al.[28] The tested film was disposed in the middle of the measurement cell composed by an upstream and a downstream chambers. First, the measurement cell containing the tested film was dried with a flow of dry nitrogen until measuring a constant dew point temperature of about −70 °C by using a chilled mirror hygrometric detector from General Eastern Instruments (USA). The nitrogen flow was then substituted by distilled liquid water (Milli-Q) in the upstream chamber, and the dew point temperature, which is directly proportional to the concentration of water molecules passing through the film thickness, was measured as a function of time in the downstream chamber. The water permeability *P* (expressed in barrer) of the films was calculated from the stationary state of the flux using the equation

DOI: 10.1021/acs.jpcc.6b11077
J. Phys. Chem. C 2017, 121, 918−930

$$P = \frac{J_{st} L}{\Delta a} \quad (1)$$

where J_{st} is the water flux at the stationary state, L is the film thickness (~250 μm), and Δa is the water activity difference between the upstream and the downstream chambers. Δa can be estimated equal to 1 since the upstream chamber was filled with liquid water, and the downstream chamber was dried with a dry nitrogen flow.

The diffusion coefficient of water molecules transferred through the tested film was calculated from the transition state by assuming

$$D = D_0 e^{\gamma C} \quad (2)$$

where D_0 is the diffusion coefficient when the water concentration tends to 0, γ is the plasticization factor, and C is the water concentration in the film. Since D is exponentially dependent with water concentration C, the D coefficient evolves during the permeation measurement. Also, an average value of D through the mean integral diffusion coefficient $\langle D \rangle$ in the film was determined as follows:

$$\langle D \rangle = \frac{1}{\Delta C} \int_{C_1}^{C_2} D(C)\, dC \quad (3)$$

where C_1 is equal to C_{eq} and C_2 can be considered equal to 0, considering the boundary conditions of permeation.

2.4.2. Liquid Water Sorption. The initial dry mass M_0 of the film was first measured on a Scaltec SBS 22 balance from Denver Instrument (USA) having a 0.01 mg resolution. Then, the tested film (20 × 20 × 0.25 mm) was rapidly putted into distilled liquid water (Milli-Q) conditioned at 25 °C. Regularly, the tested films was removed from the water and briefly sponged in order to measure its mass $M(t)$ as a function of time. The water concentration C into the tested film was calculated as follows:

$$C\ (\%) = \frac{M(t) - M_0}{M_0} \times 100 \quad (4)$$

2.4.3. Water Vapor Sorption. Water vapor sorption experiments were performed at 25 °C on an automatic dynamic vapor sorption analyzer from Surface Measurement System (United Kingdom) equipped with an electronic microbalance having a 0.1 μg resolution. After conducting a dehydration step, the film was submitted to a hydration cycle controlled by mixing dry and saturated nitrogen flows by using two mass flowmeters, which allows to control the relative humidity applied into the measurement chamber. The initial mass M_0 of the tested film was measured after the dehydration step until a constant value was reached. Then, a relative humidity (ranging from 0 to 95% RH) was applied in the measurement chamber, and the uptake of the sample mass $M(t)$ was measured as a function of the time. The concentration of water molecules C into the film sample at the t time was determined by applying the eq 4 while the concentration of water molecules in the film sample at the equilibrium state C_{eq} was determined by

$$C_{eq}\ (\%) = \frac{M_{eq} - M_0}{M_0} \times 100 \quad (5)$$

where M_{eq} is the sample mass at equilibrium state.

The water sorption isotherm, representing the water concentration at the equilibrium state C_{eq} in the film as a function of water activity a, was then plotted. The curves obtained for the different tested films were modeled using two well-known mathematical models: the Park and Feng models. Both models are appropriate to fit the isotherms curves since the deviation moduli calculated by the root sum square method (RSS method) are lower than 10%,[29] whatever the film tested, which attests to the good fitting. The Park model can be divided into three contributions reflecting a multimode sorption. At low water activities, water molecules are absorbed at the surface of specific sites called Langmuir sites. At medium water activities, the water molecule are sorbed according to the linear Henry's law, meaning that water molecules are randomly absorbed in the polymer amorphous phase. At high water activities, the water−water interactions are stronger than the water−polymer chains ones, so that aggregates of water molecules are formed. The Park model is defined by the equation

$$C = \frac{A_L b_L a}{1 + b_L a} + k_H a + n K_a k_H{}^n a^n \quad (6)$$

where A_L is the average concentration of water molecules in the Langmuir sites, b_L is the affinity constant between water molecules and the Langmuir sites, k_H is Henry's constant, K_a is the equilibrium constant associated with the water aggregation reaction, and n is the mean number of water molecules constituting the aggregates.

The Feng model, also called new dual-mode sorption (NDMS),[30] can be described from two consecutive contributions based on a multilayer sorption mode. At low water activities, water molecules are absorbed in microcavities under multilayer structure. At high water activities, as also assumed by the Park model, aggregates of water molecules are formed due to strong water molecules−water molecules interactions. The Feng model is defined as follows:

$$C = \left(C_p \frac{(A' - 1) k' a}{1 + (A' - 1) k' a} \right) + \left(C_p \frac{k' a}{1 - k' a} \right) \quad (7)$$

where C_p is the average capacity of the polymer to absorb the water molecules, A' is the difference between the microcavities and first water molecules absorbed interactions and the water molecules−water molecules absorbed in multilayer interactions, and k' is the difference between water−water interactions and the water−polymer chains interactions.

From sorption kinetics, two diffusion coefficients, related to the transfer of water molecules by random molecular motions through the films, were calculated. By assuming a constant diffusion coefficient, the solving of Fick's law (eq 8) allows to calculate the sorption advancement $M(t)/M_{eq}$ as a function of time.

$$\frac{M(t)}{M_{eq}} = \frac{4}{\sqrt{\pi}} \sqrt{\tau} \left(1 + 2\sqrt{\pi} \sum_{n=1}^{\infty} (-1)^n \operatorname{ierfc} \frac{n}{2\sqrt{\tau}} \right) = 1 - \frac{8}{\pi^2} \sum_{n=0}^{\infty} \frac{e^{-(2n+1)^2 \pi^2 \tau}}{(2n+1)^2} \quad (8)$$

The resolution of the mathematical equation allows the determination of two coefficients as a function of the extended time of the sorption process. In that case, the D_1 diffusion coefficient is related to the diffusion for short time (i.e., when $M(t)/M_{eq} < 0.5$) (eq 9) and the D_2 diffusion coefficient is for longer time (i.e., when $M(t)/M_{eq} > 0.5$) (eq 10).

DOI: 10.1021/acs.jpcc.6b11077
J. Phys. Chem. C 2017, 121, 918−930

$$\frac{M(t)}{M_{eq}} \approx \frac{4}{\sqrt{\pi}}\sqrt{\tau} \approx \frac{4}{L}\sqrt{\frac{D_1}{\pi}}\sqrt{t} \quad (9)$$

$$\ln\left(1 - \frac{M(t)}{M_{eq}}\right) \approx -\pi^2\tau - \ln\left(\frac{\pi^2}{8}\right) \approx -\pi^2\frac{D_2 t}{L^2} \ln\left(\frac{\pi^2}{8}\right) \quad (10)$$

3. RESULTS AND DISCUSSION

3.1. Unfilled PBS and PBSA Films. *3.1.1. Water Permeation.* To overcome the film thickness effect and in sake of comparison of permeation curves, the reduced water flux JL as a function of the reduced time t/L^2 was plotted (Figure 1) for the unfilled films. As usually observed in the case

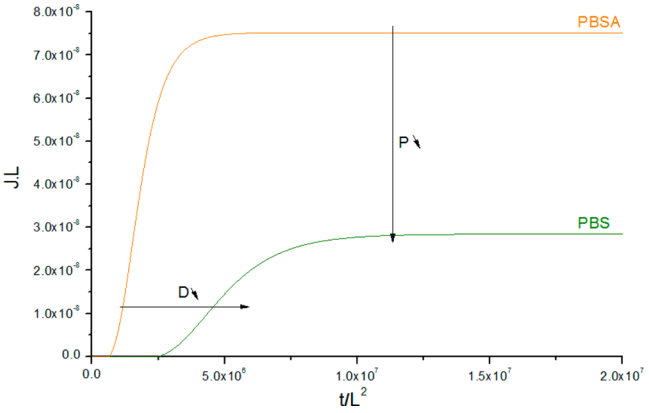

Figure 1. Reduced water permeation kinetics as a function of the reduced time t/L^2 for the unfilled PBS and PBSA films.

of water flux curves for polymer films,[31] three parts of curves can be observed. For short time, water molecules have not yet desorbed at the downstream surface of the film so that the flux J is equal to 0. When desorption of water molecules is detected at the downstream surface of the film, the J value increases until reaching a constant value, reflecting the stationary state of permeation.

From Figure 1, it is clear that the unfilled PBS and PBSA films present distinct behaviors in water permeation. The reduced water flux (Figure 1) increases earlier for the unfilled PBSA film than for the unfilled PBS film, meaning that water molecules diffuse more rapidly into the PBSA film. Also, the slope of the curve at the transient regime is higher for the PBSA film than for the PBS film, revealing a higher water diffusivity in the unfilled PBSA film. Moreover, the water flux J_{st} in film at the steady state is obtained higher for the PBSA film than for the PBS film so that the unfilled PBSA film is more permeable to water than the PBS film. The well-known plasticization phenomenon[32,33] is generally observed with water or organic vapor permeates through polymeric substrates and corresponds to Fickian behavior type B. In fact, it is usually related that the permeant concentration in a film increases during the permeation kinetic so that the number of permeant−permeant interactions increases, which leads to increase the free volume in the polymer film by swelling effects. In Figure 2a, by simulating the flux curves according to the eq 2 arising from the free volume theory, we have clearly shown the very good fitting of the experimental data for the PBS and PBSA films. Doing so, Figure 2b, presenting the water diffusivity as a function of the normalized water concentration, shows an exponential increase of the water diffusivity as the water concentration increases in both unfilled films, which reveals the plasticization phenomenon induced by water on polyester chains. In the present case, the plasticization phenomenon occurring for both films is found more pronounced in the unfilled PBSA film than in the unfilled PBS film, if we consider the higher water diffusivity in the PBSA film and its evolution with the normalized water concentration (Figure 2b). All these results are directly related to the degree of crystallinity of polyesters, which is higher for the unfilled PBS film (57% versus 37% for the PBSA film[21]). Indeed, two effects can be associated: (i) crystals are assumed to be impermeable entities inducing tortuosity effects, which slow down the transport of water molecules into a semicrystalline film, and (ii) the increase in crystallinity reduces the polymer amorphous phase, accordingly limiting the plasticization phenomena.

Being that the permeability P is directly dependent on the diffusivity as well as on the solubility of permeants into the polymer films, study the ability of our films to absorb water molecules is a required way.

3.1.2. Water Sorption. Liquid water sorption measurements were performed on the unfilled films to evaluate water solubility coefficients. Figure 3 shows the evolution of the water concentration C (deduced from the mass gain) in the unfilled

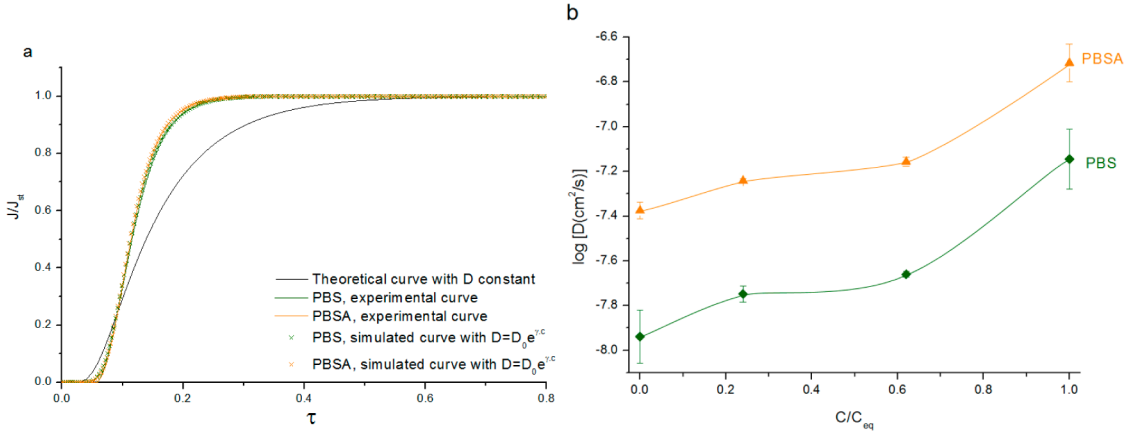

Figure 2. (a) Normalized water permeation kinetics—experimental and simulated (eq 2) curves—for the unfilled PBS and PBSA films and (b) water diffusivity as a function of the normalized water concentration C/C_{eq} in the unfilled films.

DOI: 10.1021/acs.jpcc.6b11077
J. Phys. Chem. C 2017, 121, 918−930

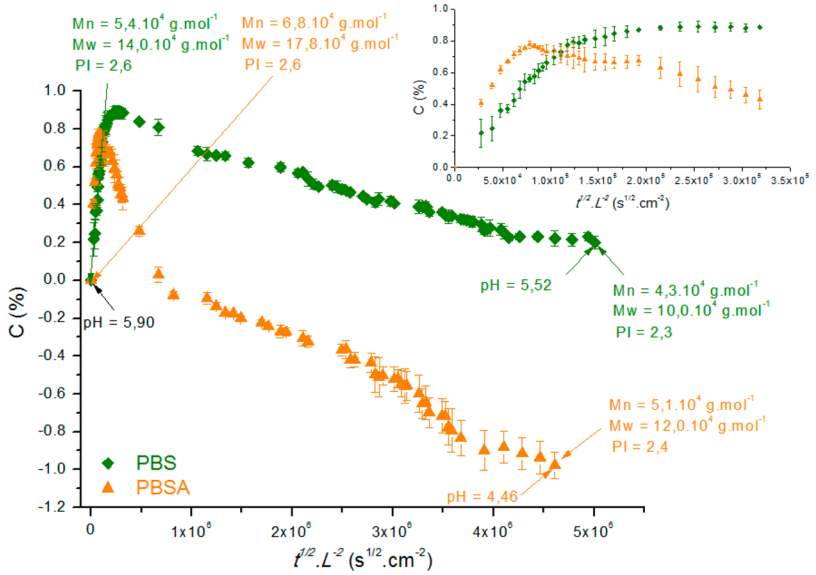

Figure 3. Liquid water sorption kinetics for the unfilled PBS and PBSA films as a function of the reduced time.

films as a function of the reduced time. The water sorption kinetics into a polymeric film are classically composed of two successive parts: absorption of water molecules by the film, which is noticed by an increase of C until a constant value is measured, reflecting the filling of all sorption sites. In our case (Figure 3), the concentration of water molecules increases for low sorption time but surprisingly a continuous decrease is measured for high sorption time for both unfilled PBS and PBSA films. However, it can be seen in the inset in Figure 3 that water molecules are absorbed more rapidly in the PBSA film than in the PBS film. Again, this result is attributed to the lower degree of crystallinity of the PBSA film compared to the PBS film. This unusual and surprising shape of sorption curves could be explained by two concomitant effects: desorption of water molecules out of the films and/or degradation of polymer chains. In order to determine the predominant effect or the concomitant action, the average molecular weights of both polyesters were measured before and after the sorption measurements. The average molecular weights of PBS and PBSA chains are reduced after sorption measurement, which reveals a degradation phenomenon of PBS and PBSA chains induced directly by liquid water, used as sorbent, through hydrolysis reactions. Moreover, another phenomenon can be reported: the pH of the aqueous solutions containing the films also decreases during the sorption course. This last result has been already observed by Phua et al.[34] and explained by hydrolysis of ester groups constituting the polymer backbones by water, which creates chains with carboxylic acid end groups and as a result solutions for sorption with lower pH values. The decrease of the sorption curves appears after about 40 min for the PBSA film and about 17.5 h for the PBS film. Moreover, the decrease of C_{eq} is significantly higher for the PBSA film than for the PBS film, meaning that PBSA is more sensitive to the degradation phenomenon. One can infer that the water molecules diffuse more rapidly in the PBSA than in the PBS so that they are larger access to the PBSA ester groups, favoring the degradation phenomenon.

In the case of the water vapor sorption measurements, any decrease of the sorbed water concentration in films was measured, even for long sorption time (500 min fixed by water activity applied). The corresponding sorption isotherms are plotted in Figure 4.

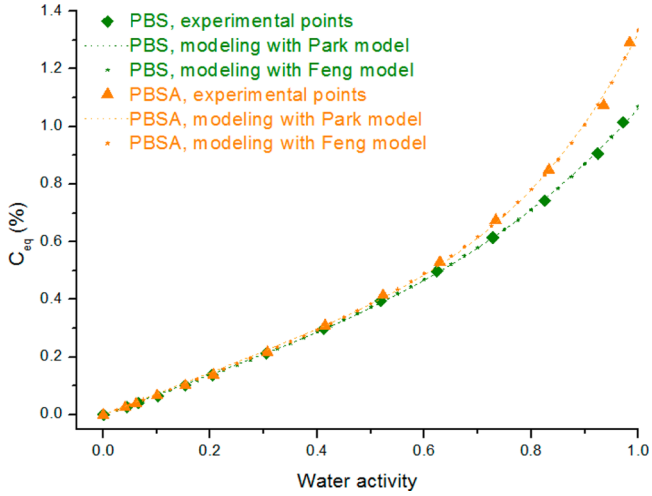

Figure 4. Water vapor sorption isotherms for the unfilled PBS and PBSA films modeled by both Park and Feng models.

The water vapor sorption behaviors of the PBS and PBSA films are found to be very similar. Only a higher sorption capacity for the PBSA film at high water activities (>0.5) was measured, which is in accordance with the degrees of crystallinity of PBS and PBSA. The experimental water sorption isotherms are successfully modeled by applying the Park and Feng models, as attested by the fitted curves reported in Figure 4 as well as by the E' values found lower than 10% (Table 1). At low water activities, the discussion about the Al and bl parameters is unsuited due to a high similarity of the sorption isotherms. Concerning the Henry's law sorption occurring at intermediate water activities, the k_H value is higher for the PBSA film: the more the water solubility in films, the more the Henry's constant. Besides, the high values of Ka and n for both PBS and PBSA films indicate the formation of water aggregates at high water activities. Water sorption occurring into the polymer amorphous phase, it is not surprising to calculate a

DOI: 10.1021/acs.jpcc.6b11077
J. Phys. Chem. C 2017, 121, 918−930

Table 1. Park and Feng Parameters for the Unfilled Films and Filled PBS- and PBSA-Based Films

	Park						Feng			
	Al (g/g)	*bl*	k_H (g/g)	K_a (g^{1-n})	*n*	*E*′ (%)	*Cp*	*A*′	*K*′	*E*′ (%)
PBSA	0.21	0.54	0.63	1.15	4.8	7.9	0.59	1.71	0.65	7.4
PBSA+CNa(5%)	0.56	0.53	0.68	1.22	5.2	9.3	0.49	2.73	0.74	8.9
PBSA+CNa(5%)-W	0.72	0.45	0.69	1.64	6.1	8.7	0.49	2.72	0.76	7.7
PBSA+C30B(5%)	1.10	0.03	0.90	0.16	5.5	6.9	0.62	2.37	0.64	6.9
PBSA+C30B(5%)-W	1.30	0.02	0.83	0.29	4.2	7.8	0.63	2.13	0.65	7.5
PBS	0.64	0.18	0.58	0.81	3.8	7.0	0.56	1.98	0.61	7.0
PBS+CNa(5%)	0.77	0.41	0.62	1.48	5.1	8.1	0.45	3.17	0.74	9.0
PBS+CNa(5%)-W	0.73	0.56	0.62	2.08	5.1	7.7	0.45	3.29	0.78	9.6
PBS+C30B(5%)	1.34	0.21	0.61	1.15	4.9	7.3	0.56	2.50	0.66	6.9
PBS+C30B(5%)-W	1.55	0.19	0.63	1.11	5.2	7.0	0.56	2.45	0.66	6.8

higher k_H value for the PBSA film than for the PBS film. Accompanied by a higher *n* value, this result means that the water aggregates are more easily formed with a larger size in the PBSA film than in the PBS film. The formation of water aggregates in the polyester films is also revealed by the values of *k*′ comprised in the Feng model, which are lower than 1, reflecting weak interactions between water and polymer chains but strong water−water interactions so that a multilayer water sorption occurs. The *A*′ parameter, relative to the water sorption on the second hydration layer of water agglomerates, is lower in the PBSA film than in the PBS film. It can be deduced a larger free volumes in the PBS film than in the PBSA film, which as a consequence facilitates the water sorption in multilayer. This result could be explained by the higher constrained amorphous phase of PBS due to its higher crystallinity and inducing a higher rigid amorphous fraction (RAF) in the PBS (X_{RAF} = 14%) than in the PBSA (X_{RAF} = 6%), as recently demonstrated,[35] which probably implies larger permanent free volumes.

The water diffusion coefficients in the unfilled PBS and PBSA films for the first-half sorption, noted *D*1, and for the second-half sorption, noted *D*2, are plotted as a function of water activity in Figure 5. It appears that both diffusion coefficients are higher for the PBSA film than for the PBS film, which is in good agreement with the water permeation results. The *D*1 coefficient seems to be constant for the whole water activity range for both unfilled films while the *D*2 coefficient is differently impacted according to the matrix. It appears

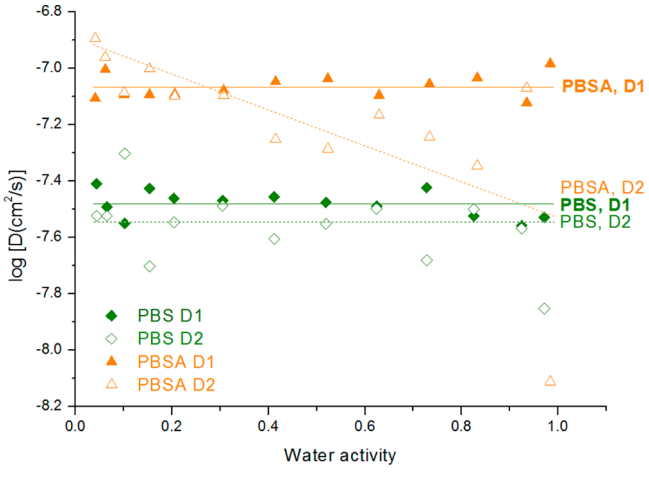

Figure 5. Evolution of the water diffusion coefficients *D*1 and *D*2 for the unfilled PBS and PBSA films.

constant for the PBS film, but it decreases for the PBSA film. In both cases, the *D*2 coefficient is found lower than the *D*1 coefficient, especially at high water concentration (high water activities). This reduction of diffusion can be directly related to the formation of water aggregates as water activity increases, which limits the water mobility and hence their diffusion within the polymer films. Considering the easier formation of water aggregates with larger size for the PBSA film, as above-mentioned, it is expected that the water mobility reduction is more marked for the PBSA films, which decreases the *D*2 coefficient.

Although the water permeability of the PBS film (*P* = 2616 barrer) and of the PBSA film (*P* = 6787 barrer) are found higher than those of others biodegradable polymers, like PLA (*P* = 1957 barrer[27]) or PHBV (*P* = 146 barrer[36]), the use of these polymers as matrices appears appropriate in the field of barrier materials by incorporating nanoplatelets. As classically reported in the literature, the dispersion and exfoliation levels are a crucial factor to achieve a reduction of water permeability and also to prevent the water absorption capacity of the resulting composite films.

3.2. PBS- and PBSA-Based Composite Films. *3.2.1. Dispersion and Exfoliation Levels of Nanofillers in Polymer Matrices.* The dispersion and exfoliation levels of the nanofillers in the two polyesters were previously detailed[23] by means of TEM observations, X-ray diffraction analyses, and rheological measurements. In the present paper, a brief report of results is proposed to evidence the clay morphology into the two matrices accompanied by TEM images given in Figure 6 and XRD spectra in Figure 7.

As recently reported,[23] the incorporation of CNa in both PBS and PBSA matrices favors the formation of filler aggregates due to the poor compatibility between CNa and the polymer chains. In other words, repulsive interactions take place between CNa and PBS or PBSA chains which prevent the polymer chains intercalation into the CNa interlayer space. By using the water-assisted extrusion process, CNa aggregates are found broken into smaller aggregates with an intercalated structure, whatever the matrix. The dispersion and exfoliation levels of C30B platelets in the PBS and PBSA-based films are clearly higher than the CNa due to the surfactant that brings a better compatibility with the matrix. Recently, a predictive approach based on a virtual materials modeling laboratory[37] was reported to probe how chemistry, combined with processing conditions, produces exfoliated clay−polymer nanocomposites in order to predict materials properties. The mechanism of clay exfoliation within a polar polymer is proposed with a relationship between the dispersion of

DOI: 10.1021/acs.jpcc.6b11077
J. Phys. Chem. C 2017, 121, 918−930

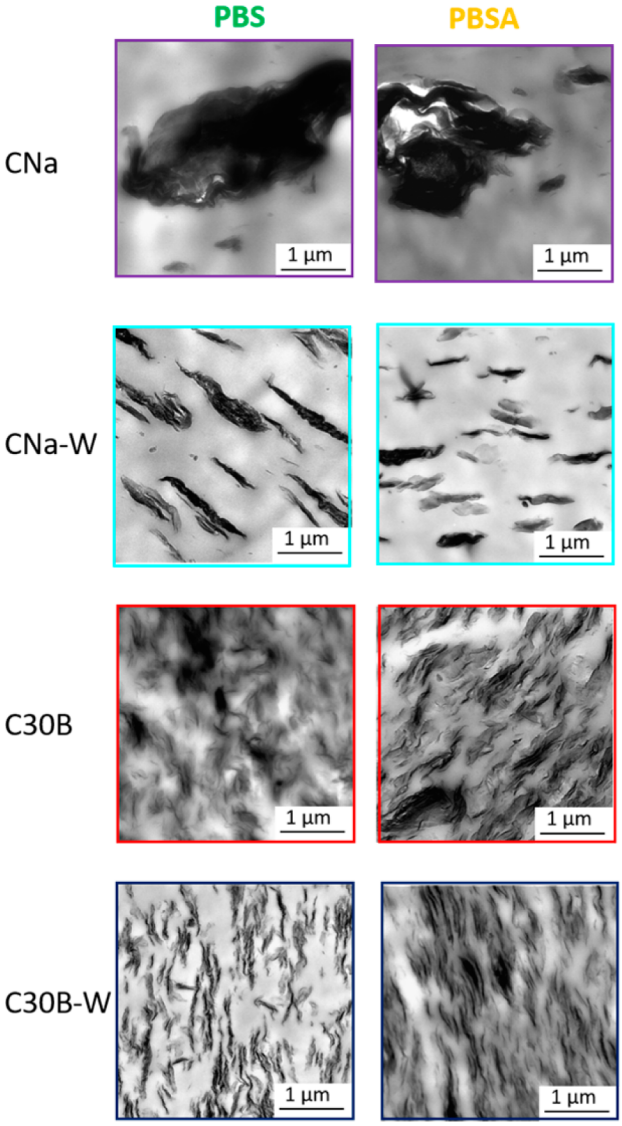

Figure 6. TEM images representative of the dispersion and exfoliation levels of fillers for the PBS- and PBSA-based composite films.

exfoliated clay platelets and the enhancement of elastic properties. The authors have reported that quaternary ammonium surfactant ions promoted exfoliation, which was dependent on grafting density of ions. In addition, the mechanism for clay exfoliation in the case of study involved layers translating parallel to one another in the most favorable case. In the present work, the difference in polarity between C30B surfactant and polymer chains is lower than between CNa and polymer chains, so that because of this higher compatibility, polymer chains can diffuse much more easily into the interlayer spaces of C30B than into CNa ones. This was also evidenced by Suter et al. In addition, Guo et al.[38] have reported that C30B can be assumed as powerful compatibilizers of the PLA/PBAT blend. The water-assisted extrusion has also differently impacted the C30B morphology according to the matrix used. Indeed, for the PBSA-based films, the C30B platelets were better dispersed and exfoliated while they are less exfoliated but more homogeneously dispersed for the PBS-based films. We believe that water molecules, injected under high pressure during extrusion process, easily diffuse between fillers and polymer chains because of the well-known

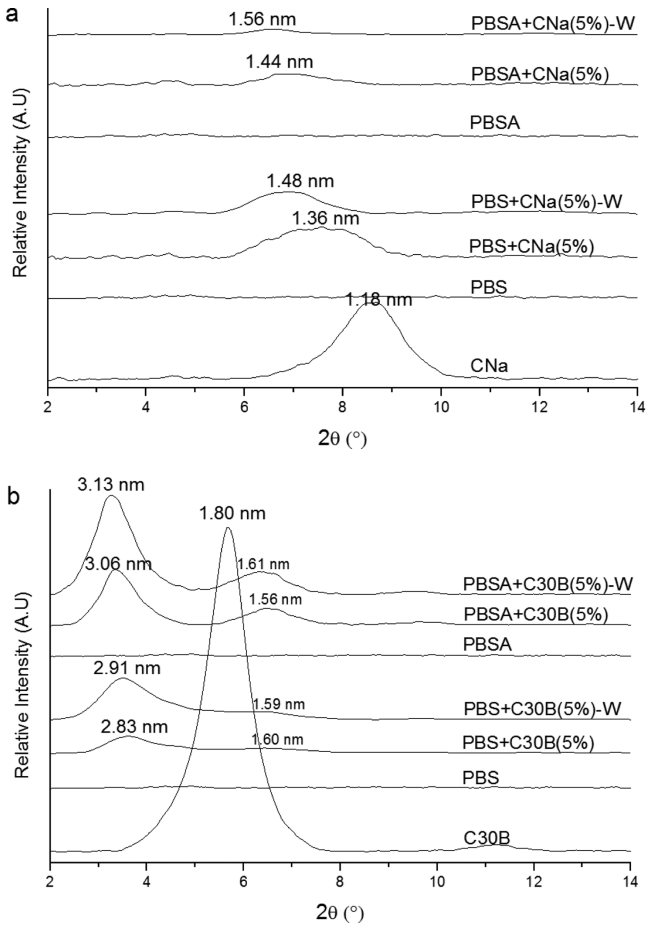

Figure 7. XRD spectra of (a) the CNa-containing composite films and (b) the C30B-containing composite films.

plasticization effect. In that case, water molecules could carry a significant amount of C30B surfactant out of the melted matter by the mean of the two degassings (atmospheric and under vacuum degassings) required during the water-assisted extrusion process. As a consequence, nanofillers could be reaggregated due to the absence of a part of C30B surfactant. Since nanofillers are only incorporated in the polymer amorphous phase, a close proximity between clays is generated for the PBS-based films having the highest degree of crystallinity (58−65%), which have strengthened the clay reaggregation phenomenon. On the contrary, for the PBSA-based films, this phenomenon has to be less present because of the higher polymer amorphous phase fraction (38−41%) which tends to increase the area devoted to fillers and hence to limit the reaggregation phenomenon.

From XRD spectra (Figure 7), the evolution of the clay basal distances as a function of clays (CNa or C30B) and of the process confirms the TEM observations. Indeed, the clay basal distances are higher for the C30B-containing nanocomposites than for the CNa-containing nanocomposites: the C30B clays are better dispersed and exfoliated than the CNa clays. It can be also observed that the water-assisted extrusion process has favored the dispersion of the CNa into all the composite films with respect to the increase of the CNa basal distance. For the C30B clays, an improvement of dispersion and exfoliation levels was noted into the PBSA-based films and also in the PBS-based films, but to a lesser extent, given the C30B basal distances. In addition, a second diffraction peak appeared at $2\theta = 6.4°$ for

DOI: 10.1021/acs.jpcc.6b11077
J. Phys. Chem. C 2017, 121, 918−930

only the C30B-containing composite films. This peak was already assigned to a second intercalated structure with lower interlayer space and was probably due to the degradation of the C30B surfactant[39] and/or platelet reagregation due to the close proximity of the interlayer distances, even using water injection. This last result is complementary to TEM observations. One can infer that C30B clays are more dispersed and exfoliated into both matrices than CNa ones. Because of a confinement effect in the highest crystalline matrix (that is PBS) causing reagregation of clays (probably due to the surfactant removal during the assisted process), the interlayer distances of C30B were found lower than in PBSA matrix. And this trend was maintained when applying the water-assisted extrusion process, as shown by the higher peak amplitudes. The water injection under high pressure and high temperature in the barrel extruder allows much greater separating the C30B nanoplatelets compared to the CNa clays, but this finding is dependent on the clay exfoliation/dispersion level already achieved by the application of classical extrusion process and on the crystallinity degree of the matrix.

3.2.3. Water Permeation. Figure 8 represents the reduced flux of water molecules JL as a function of reduced time t/L^2.

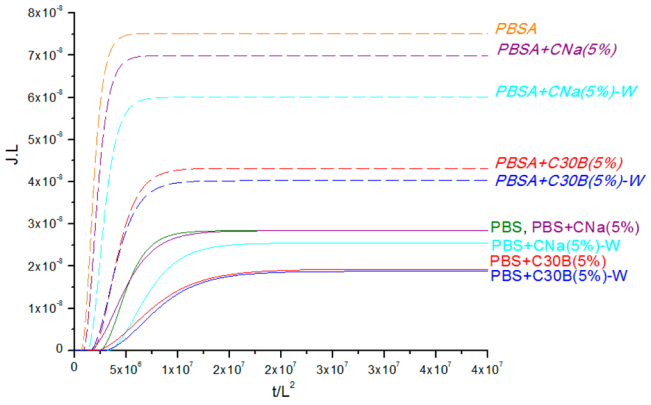

Figure 8. Reduced water flux as a function of reduced time for the PBS- and PBSA-based composite films.

The incorporation of nanofillers (CNa and C30B) in the PBSA matrix leads to delay the diffusion of the water molecules into the composite films as the first part of the curves are time-shifted to higher values and also to reduce the water permeability. Since C30B platelets are more dispersed and exfoliated than CNa in the PBSA matrix, the decrease of water permeability and the diffusion delay are higher in the PBSA +C30B film than in the PBSA+CNa film. Likewise, the dispersion and exfoliation levels of both CNa and C30B are improved by applying the water-assisted extrusion process; the diffusion delay and the decrease of water permeability are higher in the films-W than in the films extruded without water injection. From Figure 9a, it appears that the water diffusivity in the PBSA-based films follows the same trends as for water permeability. Indeed, the water diffusivity in the PBSA matrix is reduced with CNa aggregates and even more reduced with C30B nanoplatelets. The water-assisted extrusion process allows to reduce the water diffusivity for the PBSA-based composite films. Therefore, the barrier properties to liquid water of the PBSA-based films are mostly dependent on the dispersion and exfoliation levels of the fillers. In other words, tortuosity effects induced by the more or less exfoliated and

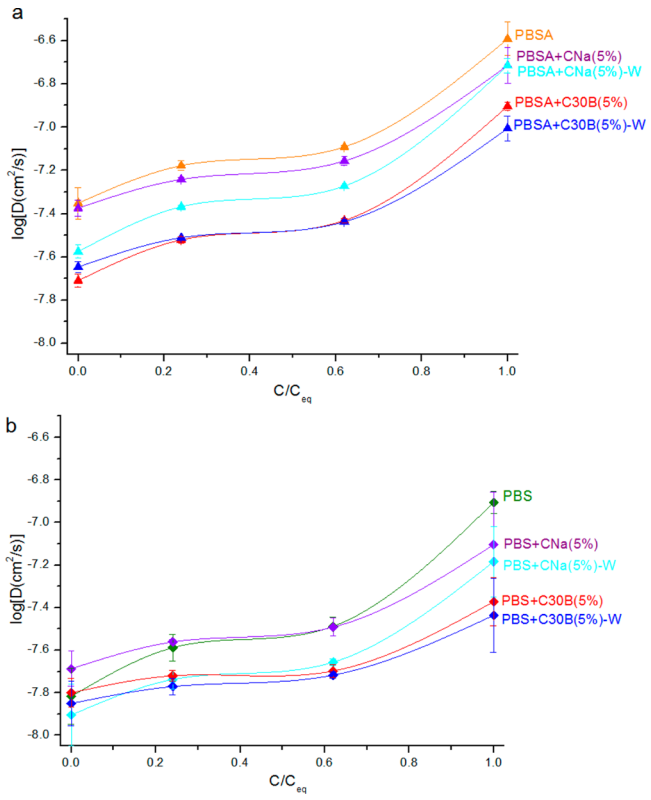

Figure 9. Evolution of the water diffusivity as a function of normalized water concentration for the PBSA-based films (a) and the PBS-based films (b).

dispersed fillers are directly responsible for the water barrier performances of the PBSA-based films.

Regarding the water permeation data for the loaded PBS films (Figure 8), it is worth noting that the evolution of the water permeability did not follow the same change as for the PBSA-based films. Indeed, the introduction of CNa in the PBS matrix seems to do not have significant effects either on the water permeability or on the diffusion. However, a decrease of the water diffusivity (Figure 9b) is noticed at high water concentrations for the PBS+CNa film(s) (i.e., when $C/C_{eq} > 0.5$) compared with the unfilled PBS film. One can assume that at low water concentrations in the PBS-based films (i.e., when $C/C_{eq} < 0.5$) CNa aggregates induce small tortuosity effects so that the water diffusivity is not or very little affected. At high water concentrations, water molecules may be in an aggregated form, which implicitly increases the permeant size. Tortuosity effects induced by CNa aggregates have to be also more important against water aggregates than against free water molecules, which diffuse more easily in the film. As expected, the incorporation of C30B leads to increase the delay time to the diffusion of water molecules and to decrease the water permeability of the PBS+C30B films compared to the PBS +CNa films due to higher dispersion and exfoliation levels of C30B platelets than CNa. The water-assisted extrusion process on the PBS+CNa-W film has significantly shifted water diffusion delay and decreased the water permeability because of the fragmentation of the CNa agglomerates which leads to increase much more tortuosity effects.

The water-assisted extrusion process has not so much effect on the water barrier properties of the PBS+C30B-W film. Indeed, the water permeability is rather similar to that of the

DOI: 10.1021/acs.jpcc.6b11077
J. Phys. Chem. C 2017, 121, 918−930

PBS+C30B film; however, a slight diffusion delay time can be observed (Figure 8). In other words, despite the fact that C30B dispersion in PBS is already fine with the use of the classical extrusion, the help of water injection allows a better dispersion of C30B in the PBS film, but to a lesser extent compared to CNa, and that would be at the origin of this slight enhancement of tortuosity effects inducing a small decrease of the water diffusivity.

The water permeation measurements have highlighted significant differences in the water permeability and the water diffusivity depending on the composition of the film and the elaboration process. In order to complete these results, water vapor sorption measurements were performed to evidence water plasticization effects.

3.2.2. Water Vapor Sorption. Water vapor sorption isotherms of fillers (CNa and C30B powder), the unfilled films, and the 5 wt % fillers-loaded films are plotted in Figure 10.

Figure 10a shows a higher water sorption for both clays than for the two polyester films directly due to the inherent hydrophilicity of clay structure. Regarding clays, the water sorption is lower in the case of C30B because of the apolar nature of the C30B surfactant. As a consequence, the water sorption is directly higher for the CNa-loaded films compared with the unfilled films and to a lesser extent for the C30B-loaded films (Figure 10b,c). The use of the water-assisted extrusion process increases the C_{eq} values in both PBS+CNa-W and PBSA+CNa-W films compared with the PBS+CNa and PBSA+CNa films, respectively. The CNa aggregates being strongly fragmented in the films-W (Figure 6), the clay surface is accordingly higher in the films extruded with water injection than in the film extruded without water injection. Water molecules are preferentially absorbed at CNa surface by affinity: the more the CNa surface, the more the water molecule sorption.

The effects of the water-injection extrusion process on the PBS+C30B-W and PBSA+C30B-W films are found to be less marked than for the PBS+CNa-W and PBSA+CNa-W films. Indeed, very similar isotherm curves are obtained between the PBS+C30B and PBS+C30B-W films whereas a higher water sorption is measured for the PBSA+C30B-W film compared with the PBSA+C30B film, especially for high water activities. Again, these results are correlated with the dispersion and exfoliation levels of fillers in the polymer matrices. Indeed, for the PBSA films (Figure 10b), the water injection during extrusion process contributes to a positive effect on the C30B exfoliation for the PBSA+C30B-W film, which induces more preferential absorption sites (on clay surface) to water molecules, by comparison with the exfoliation level for the PBSA+C30B film. For PBS films (Figure 10c), the water-assisted extrusion process reduces the C30B exfoliation level in the PBS+C30B-W film but at the same time increases their dispersion. From this observation and from the similar values of C_{eq} between the PBS+C30B and PBS+C30B-W films, one can assume that the clay surface in contact with water molecules is quite similar in both films.

In order to better understand the different phenomena taking place in the films during the water vapor sorption process, the sorption isotherms are fitted by applying the Park and Feng models. The corresponding parameters are gathered in Table 1. One can indicate that the mean deviation moduli E' are measured under 10% validating the fitting of experimental isotherm curves.

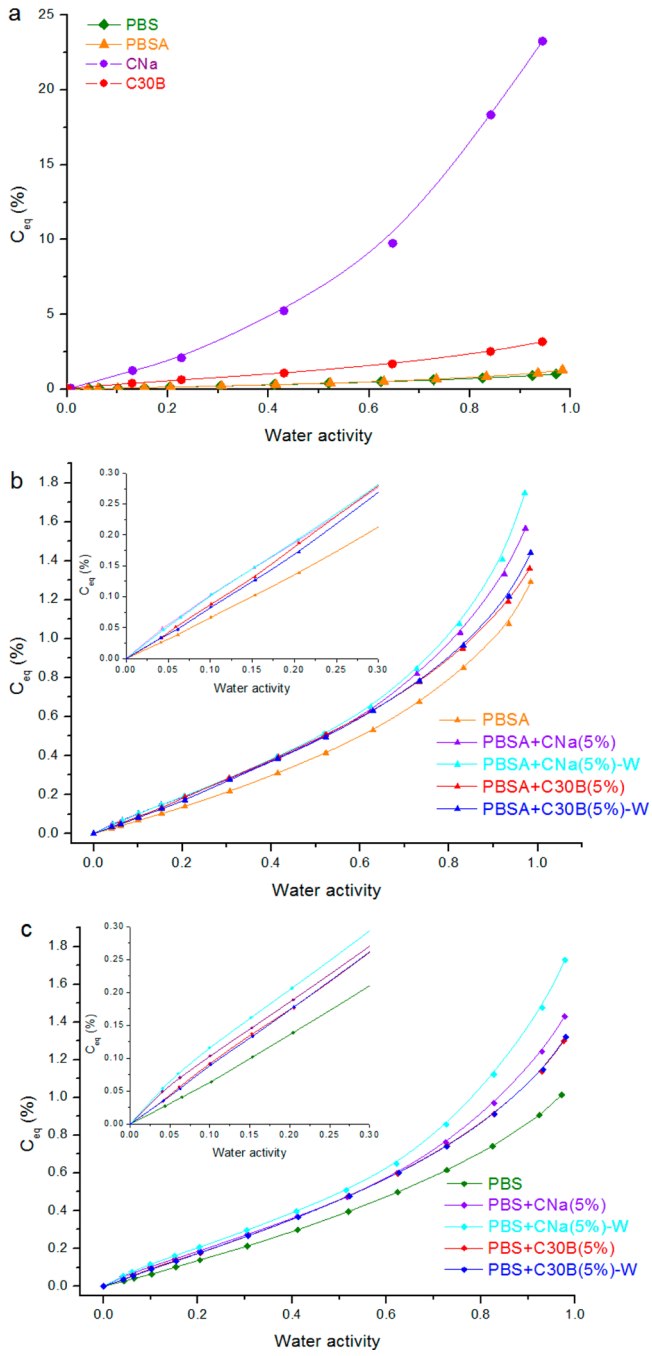

Figure 10. Water vapor sorption isotherms of (a) the fillers and the unfilled films, (b) the series of PBSA-based films, and (c) the series of the PBS-based films.

One can so infer that both models are appropriate to model the water sorption isotherms of polyester−clay films. The incorporation of CNa as well as C30B contributes to increase the *Al* parameters in both PBS- and PBSA-based films, meaning that the number of sorption sites (Langmuir sites) increases. At low water activities, water molecules are preferentially absorbed at the clay surface. The affinity between water molecules and clays is also highlighted by the high *bl* values in films filled with CNa, especially in the PBS-based films. Moreover, the low compatibility between CNa and polyester chains favors the water sorption at the clay surface. Indeed, a large amount of free volumes exist at the clay surface−polymer chains interfacial

DOI: 10.1021/acs.jpcc.6b11077
J. Phys. Chem. C 2017, 121, 918−930

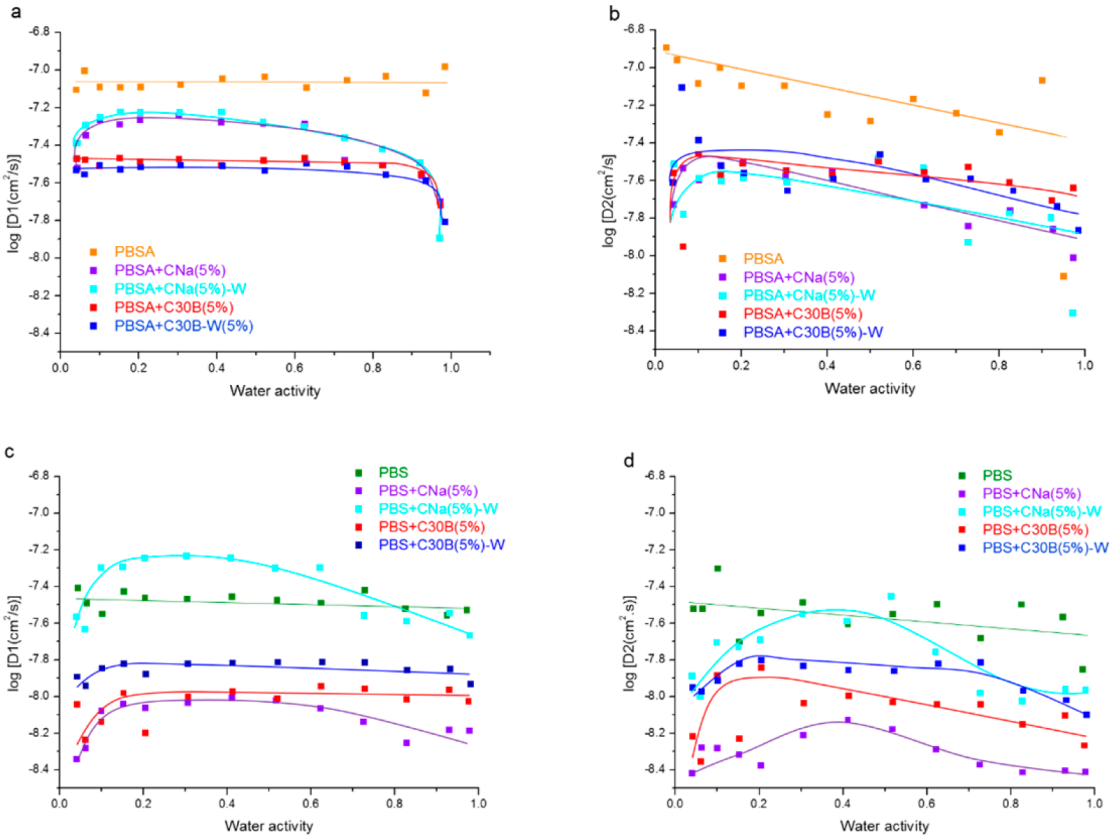

Figure 11. Evolution of the diffusion coefficients as a function of water activity.

areas, which promotes the water sorption. Concerning the C30B particles, a reduction of the *bl* values concomitant with an increase of the *Al* values is obtained if we compare with the *Al* and *bl* values for the CNa-loaded films, irrespective of matrix. It means that the affinity of water molecules with sorption sites (clay surface) decreases due to the surfactant, but at the same time, the number of sorption sites increases due to the better C30B nanoplatelet exfoliation compared with CNa.

The value of the k_H parameter is slightly higher for the composite films, especially for PBSA, meaning that the random water sorption is slightly increased in the polyester amorphous phase for intermediate water activities ($0.3 < a < 0.5$). At high water activities, CNa filler promotes the water aggregation in both PBS and PBSA matrices. Indeed, the high values of *Ka* and *n* reveal a higher water affinity into the composite films and the formation of larger water aggregates of larger size, respectively. *Ka* parameter is found lower for the C30B-loaded films than for CNa-loaded films probably due to both lower polarity and better dispersion and exfoliation of C30B nanoplatelets, which limit the water aggregation reaction. These effects are more pronounced for the PBSA-based film than for the PBS-based film. Indeed, *Ka* parameter is significantly lower for the PBSA +C30B and the PBSA+C30B-W films compared to the unfilled PBSA film, while *Ka* parameter is higher for the PBS+C30B and the PBS+C30B-W films than for the unfilled film. We speculate that the crystallinity of PBS being largely higher than that of PBSA, a close proximity between water molecules took place in the PBS film, which as a result facilitates the water aggregation reaction. Conversely, for the PBSA-based films, higher area are available to the water diffusion, which so limits the water aggregation. Since C30B platelets are found well exfoliated in the PBSA+C30B and PBSA+C30B-W films, there are numerous interaction sites between water molecules and clay platelets, which implies a better distribution of water molecules into the films and so limits the water clustering reaction.

The formation of water aggregates is facilitated with filler incorporation into the composite films, which is confirmed through the evolution of the Feng parameters. Indeed, the A' values are higher in the composite films than in the unfilled films. Moreover, the A' values, which are related to the water multilayer sorption, are higher in the CNa-loaded films than in the C30B-loaded films, which is in good agreement with the hydrophilicity inherent to CNa. At high water activities, the higher K' values found for the CNa-loaded films than for the unfilled films reveal preferential water−water interactions than water−polymer interactions. As a result, one can infer that water molecules are absorbed in multilayer at the CNa surface. For the PBS+C30B and the PBS+C30B-W films, a similar phenomenon is observed, but to a lesser extent. For the C30B-loaded PBSA films, similar K' values are obtained compared with the unfilled PBSA film, which agrees well with the sorption description deduced from the Park modeling; that is, the water aggregate formation is more difficult into the PBSA films loaded with C30B than into the PBSA films loaded with CNa.

It is difficult to thoroughly analyze the modeling parameters to directly evaluate the impacts of the water-assisted extrusion process on the water vapor sorption behavior of the corresponding films. In fact, the water sorption isotherms are very similar, whatever the extrusion conditions used, especially for the films filled with C30B. Nevertheless, some conclusions deduced from the Table 1 can be mentioned. For low water activities, the use of water injection seems to facilitate the water sorption since the *Al* values are higher for the PBS+C30B-W, PBSA+CNa-W, and PBSA+C30B-W films compared, respec-

DOI: 10.1021/acs.jpcc.6b11077
J. Phys. Chem. C 2017, 121, 918−930

tively with the PBS+C30B, PBSA+CNa, and PBSA+C30B films. This trend is in good agreement with the dispersion and exfoliation levels of fillers, as observed from TEM images. For high water activities, the *Ka* values are higher for the PBS +CNa-W and PBSA+CNa-W films than for the PBS+CNa and PBSA+CNa films, respectively. It seems also the number of water−CNa surface interactions is higher for the films-W than for those extruded without water injection, which promotes the formation of water aggregates around the CNa surface.

All these results were determined at the steady state of water vapor sorption measurements. An investigation on the behavior of sorbed water molecules during transient regime of sorption can highlight the influence of fillers and their quality of dispersion in both matrices on the water diffusivity.

Figure 11 shows the evolution of the water diffusion coefficients *D*1 and *D*2, using a semilogarithmic scale, for the composite films. It is interesting to note that *D*1 and *D*2 coefficients are in a same range of values for the whole water activity whereas it is commonly reported in the literature that the *D*2 coefficients are generally higher than the *D*1 ones[40,41] due to polymer chains plasticized by water. In our case, this result can be explained as follows: two antagonist phenomena occur into the films for longer time. The former is related to plasticization effects that can increase the water diffusivity, as observed with water permeation measurements, and the latter is the formation of water aggregates, which can decrease their mobility and hence their diffusivity. Both phenomena could explain the similarity between the diffusion values, whatever the films tested.

The incorporation of fillers (CNa and C30B) into the PBSA matrix induces significant changes on the water diffusivity in the resulting composite films. Indeed, CNa agglomerates creating small tortuosity effects; the water diffusivity is slightly decreased while for the well-dispersed/exfoliated C30B nanoplatelets inducing high tortuosity effects, the water diffusivity is strongly decreased. These results confirm again the comments related to water permeation measurements. However, contrary to results obtained with the water permeation kinetics, the water-assisted extrusion process does not seem to have significant effects on the water diffusivity for the PBSA-based films. It can be remind that the boundary conditions between water permeation and water vapor sorption measurements are different. For water permeation, only one side of the film is in contact with liquid water and the diffusivity is deduced from the water molecules transferring through the entire thickness of the tested films, while for water vapor sorption both sides of the films are in contact with water vapor and the diffusivity is the result of water molecules penetrating the film in opposite directions inside the tested film. Therefore, the measurement time is very longer for all the sorption process established at various water activities compared with the permeation process. A longer time certainly favors the formation of water clusters generally considered as a slow phenomenon. The slight difference of the water diffusivity in the PBSA-based films extruded with and without water injection is quite similar to water diffusivity from permeation results. It seems that the better dispersion of fillers due to the water injection has no real effect on the tortuosity. In fact, we can speculate that two antagonist phenomena occur into the films during sorption measurements: (i) the tortuosity induced by impermeable fillers and (ii) the creation of preferential diffusion pathways at the clay−polymer interfacial area due to the hydrophilicity of the clay (Figure 11a), which can increase the water molecule mobility. By using the water-assisted extrusion process, the dispersion and exfoliation levels of the clays are improved in composites loaded with both CNa and C30B. It results that the tortuosity effects are improved and the clay surface is also increased, so that some preferential diffusion pathways for water are created. Therefore, the very similar values of water diffusivity in the PBSA-based films extruded with and without water injection can be due to the annihilation of these antagonist effects.

For the PBS-based films, the introduction of clays also leads to decrease the diffusivity of water molecules, except for the PBS+CNa-W film. In this film, the clay (CNa) surface is important. Moreover, the compatibility between PBS chains and CNa being very poor, numerous free volumes exist at the clay−polymer chains interfacial area, which promote the preferential diffusion pathways for the diffusion of water molecules, implicitly leading to a percolation phenomenon. For the PBS+CNa film, these interfacial area are less numerous, so that the water diffusivity in this film is highly lower than for the PBS+CNa-W film. The compatibility between PBS chains and C30B is higher due to the surfactant presence, so that the number of free volumes at the vicinity of polymer chains−clays has to be significantly lower than for CNa-loaded films. Since the water diffusivity is higher in the PBS-based films loaded with C30B than loaded with CNa, a trapping effect, in addition to tortuosity effects, exists, especially with PBS having the highest crystallinity, which constraints water molecules to diffuse in a confined amorphous phase and at the vicinity of the aggregated fillers. It is now interesting to see that the water-assisted extrusion process leads to increase the water diffusivity for the PBS+C30B-W film, probably due to the better dispersion of C30B platelets. Indeed as previously mentioned, the better dispersion can lead to create preferential diffusion pathways around these hydrophilic fillers and much more when these nanoclays are present in a more confined space. One can also considered that with the use of water injection during the extrusion process, the lower exfoliation of C30B has a lesser effect on the increase of tortuosity.

4. CONCLUSION

The incorporation of 5 wt % of inorganic fillers (CNa or C30B) in a polyester matrix (PBS or PBSA) by using a water-assisted extrusion process have mainly modified the dispersion and exfoliation levels of fillers compared with the corresponding composite films classically extruded. The difference in crystallinity of matrices in addition with the change in filler structure into the matrices have strongly impacted the water barrier performances.

Both water diffusivity and solubility were found higher for the unfilled PBSA film, due to a lower crystallinity, leading to a higher water permeability. By sorption, it appears that a larger size of water aggregates has been formed in the PBSA film due to a larger polymer amorphous phase fraction. The composite films have followed the same trend, independently of extrusion conditions, because crystallinity is found in the same range than that of the unfilled films. However, the thorough analysis of the different parameters obtained in permeation and sorption measurements has allowed to identifying trends as a function of extrusion conditions and of the filler incorporated.

By applying the water-assisted extrusion process for the CNa-loaded films, a significant reduction of water diffusivity and of water permeability during permeation measurements has been evidenced because of the fragmentation of CNa aggregates promoting higher tortuosity effects. The fragmentation of the

DOI: 10.1021/acs.jpcc.6b11077
J. Phys. Chem. C 2017, 121, 918−930

CNa aggregates therefore has increased the filler surface, which has favored the water sorption preferentially. Otherwise, the C30B morphology is differently altered depending on the polyester matrix. A better exfoliation and dispersion levels of nanoplatelets is observed for the PBSA+C30B-W film than for the PBS+C30B film. This finding has been related to a reaggregation phenomenon of the platelets within a constrained amorphous phase due to the higher crystallinity of PBS. This morphology has modified the water properties so that the water permeability and the water diffusivity are quite similar between the film extruded with water injection and the film extruded without water injection. For the PBSA+C30B-W film, the water permeability and the water diffusivity are lower compared with the PBSA+C30B film due to the higher exfoliation of C30B platelets. However, the incorporation of more exfoliated fillers or of smaller filler aggregates with hydrophilic character has favored the water sorption by affinity until the formation of water aggregates at high water activities. Nevertheless, the presence of water aggregates in close proximity to fillers at the polymer/clay interfacial area has reduced the water diffusivity by trapping effects, in addition to the establishment of preferential diffusion pathways due to the increased clay surface available to water transport.

One can conclude that the filler morphology is a key factor in the improvement of water barrier performances and highly dependent on the degree of crystallinity of the matrix used and the amorphous phase more or less confined. In the present work devoted to the application of an innovative extrusion process equipped with a water injection device able to disrupt clay aggregates into a polyester matrix, the new transport properties of the resulting nanocomposites induced by the enhanced dispersion of particles were clearly explained on the basis of concomitant but antagonist effects revealed by both permeation and sorption phenomena: (i) tortuosity effects usually generated by impermeable fillers, (ii) preferential diffusion pathways promoted by an increase in clay surface or by numerous free volumes, and (iii) trapping effects owing to interactions of water aggregates developed at clay surface with hydrophilic groups.

AUTHOR INFORMATION

Corresponding Authors

*E-mail stephane.marais@univ-rouen.fr (S.M.).
*E-mail nadege.follain@univ-rouen.fr (N.F.).

ORCID

Stéphane Marais: 0000-0002-1754-1183

Notes

The authors declare no competing financial interest.

ACKNOWLEDGMENTS

The authors thank the French Ministry for the financial support of the PhD fellowship of S. Charlon.

REFERENCES

(1) Asadi, E.; Abdouss, M.; Leblanc, R. M.; Ezzati, N.; Wilson, J. N.; Kordestani, D. Synthesis, Characterization and in Vivo Drug Delivery Study of a Biodegradable Nano-structured Molecularly Imprinted Polymer based on Cross-linker of Fructose. *Polymer* **2016**, *97*, 223−237.

(2) Kumar, S.; Raj, S.; Jain, S.; Chatterjee, K. Multifunctional Biodegradable Polymer Nanocomposite Incorporating Graphene-Silver Hybrid for Biomedical Applications. *Mater. Des.* **2016**, *108*, 319−332.

(3) Touchaleaume, F.; Martin-Closas, L.; Angellier-Coussy, H.; Chevillard, A.; Cesar, G.; Gontard, N.; Gastaldi, E. Performance and Environmental Impact of Biodegradable Polymer as Agricultural Mulching Films. *Chemosphere* **2016**, *144*, 433−439.

(4) Razza, F.; Degli Innocenti, F.; Dobon, A.; Aliaga, C.; Sanchez, C.; Hortal, M. Environmental Profile of Bio-based and Biodegradable Foamed Packaging Prototype in Comparison with the Current Benchmark. *J. Cleaner Prod.* **2015**, *102*, 493−500.

(5) Habib Ullah, M.; Mahadi, W. N. L.; Latef, T. A. Aerogel Poly(butylene succinate) Biomaterial Substrate for RF and Microwave Applications. *Sci. Rep.* **2015**, *5*, 12868−12876.

(6) Thirunavukarasu, K.; Purushothaman, S.; Sridevi, J.; Aarthy, M.; Gowthaman, M. K.; Nakajima-Kambe, T.; Kamini, N. R. Degradation of Poly(butylene succinate) and Poly(butylene succinate-co-butylene adipate) by Lipase from Yeast Cryptococcus sp. Grown on Agro-industrial Residues. *Int. Biodeterior. Biodegrad.* **2016**, *110*, 99−107.

(7) Llorens, E.; Ibanez, H.; del Valle, L. J.; Puiggali, J. Biocompatibility and Drug Release Behavior of Scaffolds Prepared by Coaxial Electrospinning of Poly(butylene succinate) and Poly-ethylene glycol. *Mater. Sci. Eng., C* **2015**, *49*, 472−484.

(8) Xu, J.; Guo, B.-H. Poly(butylene succinate) and its Copolymers: Research, Development and Industrialization. *Biotechnol. J.* **2010**, *5*, 1149−1163.

(9) Kim, H.-S.; Kim, H.-J. Enhanced Hydrolysis Resistance of Biodegradable Polymers and Bio-composites. *Polym. Degrad. Stab.* **2008**, *93*, 1544−1553.

(10) Makhatha, M.; Ray, S. S.; Hato, J.; Luyt, A. S. Thermal and Thermomechanical Properties of Poly(butylene succinate) Nano-composites. *J. Nanosci. Nanotechnol.* **2008**, *8*, 1679−1689.

(11) Siracusa, V.; Lotti, N.; Munari, A.; Dalla Rosa, M. Poly(butylene succinate) and Poly(butylene succinate-co-adipate) for Food Pack-aging applications: Gas Barrier Properties after Stressed Treatments. *Polym. Degrad. Stab.* **2015**, *119*, 35−45.

(12) Fujimaki, T. Processability and Properties of Aliphatic Polyesters, 'Bionolle', Synthesized by Polycondensation Reaction. *Polym. Degrad. Stab.* **1998**, *59*, 209−214.

(13) Tan, B.; Thomas, N. L. A Review of the Water Barrier Properties of Polymer/Clay and Polymer/Graphene Nanocomposites. *J. Membr. Sci.* **2016**, *514*, 595−612.

(14) Guo, Y.; Yang, K.; Zuo, X.; Xue, Y.; Marmorat, C.; Liu, Y.; Chang, C.-C.; Rafailovich, M. H. Effects of Clay Platelets and Natural Nanotubes on Mechanical Properties and Gas Permeability of Poly (lactic acid) Nanocomposites. *Polymer* **2016**, *83*, 246−259.

(15) Picard, E.; Gérard, J.-F.; Espuche, E. Reinforcement of the Gas Barrier Properties of Polyethylene and Polyamide Through the Nanocomposite Approach: Key Factors and Limitations. *Oil Gas Sci. Technol.* **2015**, *70*, 237−249.

(16) Al-Qadhi, M.; Merah, N. Mechanical and Physical Properties of Polymer-Based Nanocomposites Containing Different Types of Clay. *Polym. Compos.* **2015**, *36*, 1998−2007.

(17) Saurabh, C. K.; Gupta, S.; Bahadur, J.; Mazumder, S.; Variyar, P. S.; Sharma, A. Mechanical and Barrier Properties of Guar Gum Based Nanocomposite Films. *Carbohydr. Polym.* **2015**, *124*, 77−84.

(18) Sallem-Idrissi, N.; Sclavons, M.; Devaux, J. Synthesis of Polymer Nanocomposites by Water-Assisted Extrusion. In *Synthesis Techniques for Polymer Nanocomposites*; Mittal, V., Ed.; Wiley-VCH Verlag GmbH & Co. KGaA: Weinheim, Germany, 2014; Chapter 8, pp 179−209.

(19) Rousseaux, D. D. J.; Sallem-Idrissi, N.; Baudouin, A.-C.; Devaux, J.; Godard, P.; Marchand-Brynaert, J.; Sclavons, M. Water-assisted Extrusion as a Novel Processing Route to Prepare Polypropylene/Halloysite Nanotube Nanocomposites: Structure and Properties. *Polymer* **2011**, *52*, 443−451.

(20) Rousseaux, D. D. J.; Sclavons, M.; Godard, P.; Marchand-Brynaert, J. Polypropylene/Clay Nanocomposites: An innovative One-Pot Process. *Polym. Compos.* **2015**, *36*, 644−650.

(21) Touchaleaume, F.; Soulestin, J.; Sclavons, M.; Devaux, J.; Lacrampe, M. F.; Krawczak, P. One-step Water-Assisted Melt-Compounding of Polyamide 6/Pristine Clay Nanocomposites: An

DOI: 10.1021/acs.jpcc.6b11077
J. Phys. Chem. C 2017, 121, 918−930

Efficient Way to Prevent Matrix Degradation. *Polym. Degrad. Stab.* **2011**, *96*, 1890−1900.
(22) Mainil, M.; Urbanczyk, L.; Calberg, C.; Germain, A.; Jerome, C.; Bourbigot, S.; Devaux, J.; Sclavons, M. Morphology and Properties of SAN-Clay Nanocomposites Prepared Principally by Water-Assisted Extrusion. *Polym. Eng. Sci.* **2010**, *50*, 10−21.
(23) Charlon, S.; Follain, N.; Chappey, C.; Dargent, E.; Soulestin, J.; Sclavons, M.; Marais, S. Improvement of Barrier Properties of Bio-Based Polyester Nanocomposite Membranes by Water-Assisted Extrusion. *J. Membr. Sci.* **2015**, *496*, 185−798.
(24) Shih, Y. F.; Wang, T. Y.; Jeng, R. J.; Wu, J. Y.; Wuu, D. S. Cross-Linked and Uncross-Linked Biodegradable Nanocomposites. I. Non-isothermal Crystallization Kinetics and Gas Permeability. *J. Appl. Polym. Sci.* **2008**, *110*, 1068−1079.
(25) Ray, S. S.; Okamoto, K.; Okamoto, M. Structure and Properties of Nanocomposites Based on Poly(butylene succinate) and Organically Modified Montmorillonite. *J. Appl. Polym. Sci.* **2006**, *102*, 777−785.
(26) Soulestin, J.; Rashmi, B. J.; Bourbigot, S.; Lacrampe, M.-F.; Krawczak, P. Mechanical and Optical Properties of Polyamide6/Clay Nanocomposite Cast Films: Influence of the Degree of Exfoliation. *Macromol. Mater. Eng.* **2012**, *297*, 444−454.
(27) Tenn, N.; Follain, N.; Soulestin, J.; Crétois, R.; Bourbigot, S.; Marais, S. Effect of Nanoclay Hydration on Barrier Properties of PLA/montmorillonite Based Nanocomposites. *J. Phys. Chem. C* **2013**, *117*, 12117−12135.
(28) Alexandre, B.; Langevin, D.; Mederic, P.; Aubry, T.; Couderc, H.; Nguyen, Q. T.; Saiter, A.; Marais, S. Water Barrier Properies of Polyamide 12/montmorillonite Nanocomposite membranes: Structure and Volume Fraction Effects. *J. Membr. Sci.* **2009**, *328*, 186−204.
(29) Lomauro, C. J.; Bakshi, A. S.; Labuza, T. P. Evaluation of Food Moisture Sorption Isotherm Equations - Part I. Fruit, Vegetable and Meat-Products. *Lebensm. Wiss Technol.* **1985**, *18*, 111−117.
(30) Feng, H. Modeling of Vapor Sorption in Glassy Polymers Using a New Dual Mode Sorption Model Based on Multilayer Sorption Theory. *Polymer* **2007**, *48*, 2988−3002.
(31) Metayer, M.; Labbé, M.; Marais, S.; Langevin, D.; Chappey, C.; Dreux, F.; Brainville, M.; Belliard, P. Diffusion of Water Through Various Polymer Films: a New High Performance Method of Characterization. *Polym. Test.* **1999**, *18*, 533−549.
(32) Matveev, Y. I.; Grinberg, V. Y.; Tolstoguzov, V. B. The Plasticizing Effect of Water on Proteins, Polysaccharides and their Mixtures. Glassy State of Biopolymers, Food and Seeds. *Food Hydrocolloids* **2000**, *14*, 425−437.
(33) Shahid, S.; Nijmeijer, K. Performance and Plasticization Behaviour of Polymer-MOF Membranes for Gas Separation at Elevated Pressures. *J. Membr. Sci.* **2014**, *470*, 166−177.
(34) Phua, Y. J.; Chow, W. S.; Mohd Ishak, Z. A. The Hydrolytic Effect of Moisture and Hygrothermal Aging on Poly(butylene succinate)/organo-montmorillonite Nanocomposites. *Polym. Degrad. Stab.* **2011**, *96*, 1194−1203.
(35) Charlon, S.; Marais, S.; Dargent, E.; Soulestin, J.; Sclavons, M.; Follain, N. Structure-Barrier Property Relationship of Biodegradable Poly(butylene succinate) and Poly((butylene succinate)-co-(butylene adipate)) Nanocomposites: Influence of the Rigid Amorphous Fraction. *Phys. Chem. Chem. Phys.* **2015**, *17*, 29918−29934.
(36) Crétois, R.; Follain, N.; Dargent, E.; Soulestin, J.; Bourbigot, S.; Marais, S.; Lebrun, L. Microstructure and Barrier Properties of PHBV/organoclays Biocomposites. *J. Membr. Sci.* **2014**, *467*, 56−66.
(37) Suter, J. L.; Groen, D.; Coveney, P. V. Mechanism of Exfoliation and Prediction of Materials Properties of Cvlay-polymer Nanocomposites from Multiscale Modeling. *Nano Lett.* **2015**, *15*, 8108−8113.
(38) Guo, Y.; He, S.; Yang, K.; Xue, Y.; Zuo, X.; Yu, Y.; Liu, Y.; Chang, C.-C.; Rafailovich, M. H. Enhancing the Mechanicanl Properties of Biodegradable Polymer Blends using Tubular Nanoparticle Stitching of the Interfaces. *ACS Appl. Mater. Interfaces* **2016**, *8* (27), 17565−17573.
(39) Yoon, P. J.; Hunter, D. L.; Paul, D. R. Polycarbonate nanocomposites. Part 1. Effect of Organoclays Structure on the Morphology and Properties. *Polymer* **2003**, *44*, 5323−5339.
(40) Follain, N.; Belbekhouche, S.; Bras, J.; Siqueira, G.; Marais, S.; Dufresne, A. Water Transport Properties of Bio-nanocomposites Reinforced by Luffa Cylindrica Cellulose Nanocrystals. *J. Membr. Sci.* **2013**, *427*, 218−229.
(41) Alix, S.; Philippe, E.; Bessadok, A.; Lebrun, L.; Morvan, C.; Marais, S. Effect of Chemical Treatments on Water Sorption and Mechanical Properties of Flax Fibres. *Bioresour. Technol.* **2009**, *100*, 4742−4749.

DOI: 10.1021/acs.jpcc.6b11077
J. Phys. Chem. C 2017, 121, 918−930